ARTICLE

An Investigation on the Capillary Wetting of Glass Fiber Tow and Fabric Structures with Nanoclay-Enriched Reactive Epoxy and Silicone Oil Mixtures

Ayça Ertekin,*,†,§ Sadhan C. Jana,† and Richard R. Thomas*,‡

Department of Polymer Engineering, The University of Akron, Akron, Ohio 44325-0301, and OMNOVA Solutions Inc., 2990 Gilchrist Road, Akron, Ohio 44305-4418

ABSTRACT Capillary wetting of a biaxially-oriented glass fabric and the tow comprising the fabric was examined via the Washburn equation with silicone oil and a reactive epoxy-curative system containing 0−4 wt % nanoclay reinforcement. Capillary wetting of silicone oil was used to measure the hydraulic constant of the fabric and tow. The wetting rates for fabric were found to be greater than those for tow and this was based on the larger pore radii of fabric compared to tow. Reynolds and capillary numbers calculated from wetting rate data indicated that the flow is dominated by interfacial tension. The presence of nanoclay offered a significant perturbation to capillary wetting behavior. Wetting rates indicate that the effect of nanoclay is 2-fold: blocking of tow pores and increasing the wetted area. This suggests that nanoclay particles are aggregating and the flow field is such that the particles are not dispersed additionally under the present conditions. Capillary wetting rates of fabric and tow samples were measured with reactive epoxy-amine mixtures at various nanoclay loadings. The presence of nanoclay offers another level of complexity to the Washburn equation. In addition to the liquid/fabric or tow interfacial tension, the interfacial tension of the liquid/nanoclay interface has to be reconciled. As a consequence, hydraulic constant, surface tension, and contact angle are convoluted in such a binary system.

KEYWORDS: Capillary wetting • nanoclay • resin transfer molding

INTRODUCTION

Epoxy resins are one of the most versatile and easy to use thermoset resins available in the market because of their relatively high tensile strength, good chemical resistance, and low shrinkage characteristics upon molding. They can be tailored to be compatible with a wide range of processing techniques, ranging from pultrusion, injection molding, and solid tape laying to resin transfer molding (RTM). Traditional RTM is a liquid composite molding technique preferred for high performance, high volume, low cost, and net shape manufacturing of a variety of polymer composites. RTM entails injection of a reactive resin system into a closed mold-cavity already preloaded with a fabric reinforcement that is subsequently cured to obtain the desired component. The process and advantages of RTM have been discussed by many researchers extensively (1−6). With the developments in nanoscience and nanotechnology, the feasibility and potential benefits of adding nanoreinforcements, such as nanoclay and carbon nanotubes, into epoxy systems have been reported recently by a few researchers. A majority of these studies are focused on investigating synergistic effects of nanoreinforcements on the mechanical and thermal properties of multiscale reinforced composites (7−13).

Wetting of fiber reinforcements by resin systems is one of the major concerns directly influencing impregnation, adhesion, and final properties of composites during RTM. The flow and wetting of epoxy resins in glass-reinforced systems have been the subject of numerous investigations (5, 14−22). Typically, a fabric system is comprised of many tows, each of which consists of many individual fibers; therefore, the fabric alone is expected to exhibit multiscale wetting behavior. Incorporation of a nanoreinforcement into a resin offers another perturbation to the wetting and flow of resin around the glass fabric, the effects of which still remain to be investigated thoroughly.

Whether a reactive thermoset resin system impregnates a porous fiber reinforcement system effectively depends on viscosity, surface tension, and contact angle characteristics. A proper match of the surface properties of resins to those of reinforcements is one of the key issues in achieving successful wetting during RTM and realizing best composite properties. As capillary wetting is a result of surface forces, an evaluation of surface tension properties is crucial. Typically, a combination of low values of surface tension and viscosity of the resin is desired for good fiber impregnation.

The analysis of wettability of reactive resin systems is an area requiring further investigation because of the complexities involved not only in the evaluation of capillary wetting but also in the determination of surface tension and viscos-

* Corresponding author.
Received for review March 17, 2009 and accepted July 13, 2009
† The University of Akron.
‡ Omnova Solutions Inc.
§ Current address: DNV Research & Innovation USA, 5777 Frantz Road, Dublin, Ohio 43017-1386.
DOI: 10.1021/am900179x

Published on Web 08/04/2009

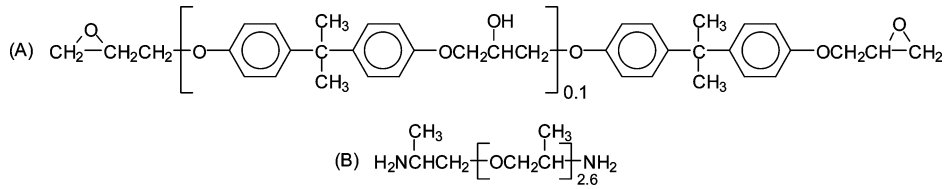

FIGURE 1. Structures of (A) DGEBA epoxy monomer (Epon 828) and (B) diamine curing agent (Jeffamine D-230).

ity, whereas curing reactions take place in reactive resin systems (23). A fundamental understanding of the differences in wetting of fibrous reinforcements, when subjected to various nanoclay-enriched reactive resin systems, is essential through an assessment of capillary wetting. The Washburn equation is one of the most commonly used approaches in evaluating wetting characteristics of porous solids, powders and fibrous materials (24). Washburn theory (25) proposes that when a porous material is brought into contact with a liquid, capillary pressure causes the liquid to enter pores under proper conditions.

In this research, the relative importance of interfacial forces over viscous forces and wettability of biaxially-oriented E-glass fibers with nanoclay-reinforced epoxy resins was assessed by capillary wetting experiments measuring impregnation rate and impregnation height as well as viscosity and surface tension of the resin. During traditional RTM of woven or stitched fabrics, the resin is forced to flow into two regions: gaps among individual filaments in a tow (intratow) and gaps between the fiber tows (intertow) (26). The objective of studying the wetting properties of such porous glass fabrics and tows was to gain an understanding of the effects of curative and nanoclay particles on the control of wettability and to assess the feasibility of flow through such porous media in the presence of complex nanoreinforced epoxy systems in RTM applications. The relative magnitudes of the factors affecting resin and curative adsorption kinetics of such complex, multicomponent, reactive epoxy mixtures were also evaluated. It was hypothesized that the diamine curative interacted with the nanoclay, as reported elsewhere (23, 27).

The dimensions of flow channels between intratow and intertow regions of a fabric differ by 2−3 orders of magnitude. This usually leads to nonuniform microflow and macroflow fields depending on processing parameters such as injection pressure, flow rate in RTM, and capillary forces. As a consequence, void formation can arise during the mold-filling stage of RTM. This is also reflected in the capillary numbers observed commonly during RTM. Several researchers (15, 28) reported a critical capillary number range between 2×10^{-4} and 2.5×10^{-3}, below which severe void problems are observed during RTM. In this study, capillary numbers obtained from capillary wetting measurements of nanoclay-reinforced reactive epoxy mixtures with both tow and fabric samples were found to be much smaller than 1 suggesting a strong potential for void formation. Indeed, these expectations were supported by several optical micrographs taken from various cross-sectional areas of RTM molded composites and inferred from reduction of mechanical properties of composites. This will be the subject of a subsequent publication. All of these results served to emphasize the relative importance of capillary effects and viscosity during impregnation of nanoreinforced epoxy systems.

EXPERIMENTAL SECTION

Raw Materials. A diglycidyl ether of bisphenol A (DGEBA), Epon 828, aromatic epoxy resin system with a viscosity of 11−15 Pa·s, an equivalent weight of 178−190 and a specific gravity of 1.15 g/mL at 25 °C was obtained from Miller Stephenson Chem. Inc. (Danbury, CT) because of its utility in liquid composite molding applications. A polyoxypropylene, aliphatic diamine curing agent, Jeffamine D-230, with a nominal molecular weight of 225 g/mol and a viscosity of 1.04×10^{-2} Pa·s at 25 °C was purchased from Huntsman Inc. (Houston, TX). The chemical formula of both epoxy and curative are illustrated in Figure 1, A and B, respectively. A Dow Corning 200 poly(dimethylsiloxane) fluid with a surface tension of 19.7 mN/m, a specific gravity of 0.915 g/mL and a viscosity of 4.58×10^{-3} Pa s was used to determine the hydraulic constant of glass fabrics and single tows during some of the capillary wetting experiments. Nanomer I.30E, an octadecyl ammonium ion-modified montmorillonite clay, with a density of 1.71 g/cm^3 was obtained from Nanocor Inc. Nanomer I.30E nanoclay is reported to be comprised of 70−75 wt % montmorillonite and 25−30 wt % octadecylamine. The CD 185A biaxially stitched E-glass fabric was purchased from Owens Corning. This fabric was selected due to its rapid wetting, good processing and mechanical properties for RTM experiments. The fabric was made of tows perpendicular to each other (0° and 90° orientation) with a fabric weight of 630 g/m^2. The tows were held together with polyester knitting. Owens Corning claimed that an aminosilane sizing agent was applied to the tows of this fabric to improve the fiber−matrix compatibility, processability, fiber strength, wetting, and handling. It was also reported by Owens Corning that the CD 185A fabric was made from SE 1200−675 yield (735 tex) rovings with 2000 filaments/tow and with a single filament diameter of ~13 μm designed specifically for epoxy resin systems.

Capillary Wetting Measurements. Capillary wetting experiments of biaxially-oriented E-glass fabrics and single tows was conducted with various wetting fluids. For this purpose, an experimental apparatus comprised of a high precision (±0.1 mg) Ohaus Adventurer AR 1140 microbalance, a laboratory jack and a PC running data acquisition software (ScaleSoft Development Corp.) was built. Both rectangular fabric samples of 0.52 mm × 20 mm × 50 mm and single tow samples of 0.52 mm × 2 mm × 120 mm were tested. Silicone oil, silicone oil−nanoclay, epoxy-curative, and epoxy-curative−nanoclay mixtures were used as the wetting fluids. Disperson of any additive in a resin is a substantial concern because the nanomaterials, as-supplied, are usually aggregated. For the preparation of epoxy−nanoclay test fluids, all materials were vacuum-dried at 80 °C for 12 h prior to capillary wetting measurements. A calculated amount of nanoclay was first mixed with epoxy at 80 °C for 2 h using a 700-W, 1 HP high-shear laboratory mixer Omni GLH-115 model homogenizer from OMNI Inc., operating at 10 000 rpm. The resultant mixture was then cooled to 25 °C and sonicated for 15 min in an ice-bath using a MISONIX S-3000 sonicator with

a 600 W generator, 20 kHz converter and 3/4 in. tapped horn. After sonication, the mixture was cooled to 25 °C and degassed for 20 min. For preparation of reactive epoxy−clay test fluids, a stochiometric amount of curative was next mixed thoroughly with epoxy−clay mixtures at room temperature. The same procedure, except for addition of curative, was followed during the preparation of silicon oil−clay samples.

During capillary wetting measurements, a test fabric sample was attached to a thin metal wire and the assembly was suspended beneath the microbalance such that the fabric remained parallel with the wetting liquid surface. After the microbalance was tared, the test liquid was raised until it contacted the fabric or tow specimen and data collection commenced. Data collection was terminated when the wetting rate ceased to change with time. Three data sets were collected for each sample condition. Variance in calculated values of hydraulic constants and wetting rates represent propagation of errors. These are coupled with errors obtained from linear-least-squares fitting of data over the steady-state region.

Surface Tension Measurements. The surface tensions of both unreactive and reactive epoxy-nanoclay mixtures were measured using a Du Nouy Ring tensiometer (Fisher Surface Tensiomat Model 21) from Fisher Scientific. Data from surface tension measurements were corrected via the Zuidema−Waters equation (29).

Viscosity Measurements. A TA Instruments AR 2000 rheometer with a "cup and bob" geometry was used to measure viscosities at controlled strain. The sample preparation conditions were similar to those used for capillary wetting measurements. After placing the test fluids into a cup and raising the cup into position, the TA rheometer was allowed to equilibrate for 1 min. The viscosities of all test liquid mixtures were measured every 10 s, whereas the shear rates ranged from 0.01 to 100 s^{-1} at intervals of 5 points per decade.

Density Measurements. Because of the difficulty of cleaning highly viscous, reactive epoxy mixtures, density measurements using a pycnometer were not practical. Density measurements of all reactive and nonreactive epoxy and epoxy−nanoclay mixtures were conducted using a 4 mL graduated cylinder that was cut from a 10 mL graduated cylinder. A sample size of 3 mL of each test fluid was poured carefully into a tared, graduated cylinder, avoiding any bubbles, and then weighed with a high precision balance. Density measurements were repeated at least five times for each material system to estimate errors due to meniscus readings.

Scanning Electron Microscopy (SEM) and Energy-Dispersive Spectrometry (EDS) Measurements. The microstructure of cured (80 °C, 2 h; 125 °C, 3 h) samples of epoxy−glass fabric−nanoclay samples was examined by a JEOL 840-A SEM equipped with a Bruker X-Flash 4010 energy dispersive spectrometer (EDS) using Quantax 200 software. The SEM was operated at 15 keV. The cured samples of epoxy−glass fabric−nanoclay were prepared by standard metallographic techniques. The polished samples were carbon coated.

RESULTS AND DISCUSSIONS

The epoxy-curative system chosen for study comprised a DGEBA epoxy monomer (Epon 828) and diamine curing agent (Jeffamine D-230). The structures of the compounds are shown in Figure 1. The chemistry and curing of epoxy−amine resins has been well-documented and will not be discussed here further (30). For an actual RTM part, heat is applied after the mold has filled to ensure complete curing. Curing does not occur to any appreciable extent, vide infra, over the course of capillary wetting measurements.

A plan view optical image of the biaxially oriented fabric is shown in Figure 2A, whereas a SEM cross-sectional image

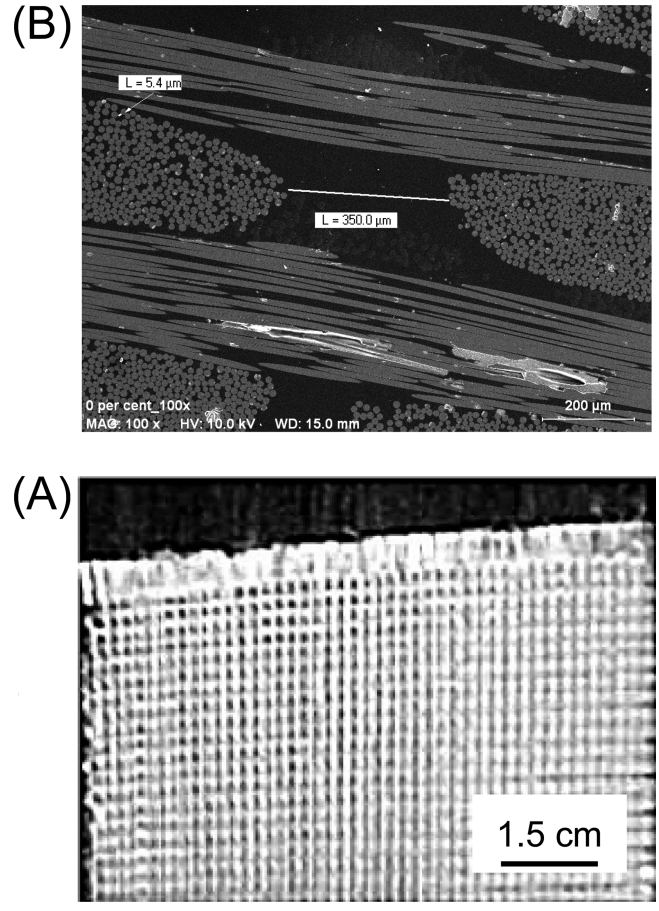

FIGURE 2. Biaxially oriented, CD 185A glass fiber fabric: (A) plan view of the fabric observed under optical microscopy and (B) cross-sectional image obtained by SEM.

provided in Figure 2 B shows the distribution of inter- and intratow regions in a fabric. The incompatibility between surface properties of resins with those of reinforcements is one of the greatest concerns in resin transfer molding (RTM) applications. Consequently, wetting of fibrous structures and its influence on viscous/capillary flows in tows or fabrics, and ultimately on void entrapment mechanisms, play a critical role in the success of RTM.

Wettability of fibrous reinforcements, particularly with nanoparticle-modified resin systems, is an area where a scarcity of published research studies is available. In this study, the effects of nanoclay-modified epoxy systems on the wetting of glass fiber reinforcement systems were examined via Washburn-type capillary wetting experiments (25) with an emphasis on changes in tow and fabric axial resin impregnation rates and other surface properties.

The analysis of capillary flow through porous media can be described by the Washburn equation (31)

$$m^2 = \frac{R_c \rho^2 \gamma \cos\theta}{2\mu} t \qquad (1)$$

where m is mass, R_c is the hydraulic constant, ρ is liquid density, γ is liquid surface tension, θ is the contact angle of the liquid with the fabric, t is time, and μ is dynamic

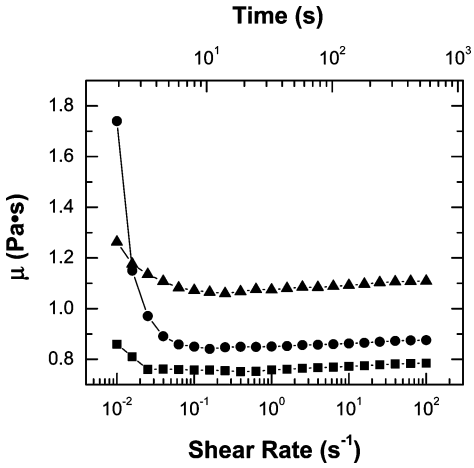

FIGURE 3. Viscosity of reactive epoxy-curative mixtures containing 0 (■), 2 (●), and 4 (▲) wt % nanoclay measured at 25 °C as a function of time and shear rate.

viscosity. The hydraulic constant, R_c, can also be expressed as a function of the wetted area, A, capillary (hydraulic) radius, r, and the number of capillaries, n_k, as follows

$$R_c = A^2 r = \frac{n_k^2 \pi^2 r^5}{2} \qquad (2)$$

Washburn theory suggests that when a porous test material, such as a glass fiber tow or fabric, is brought into contact with a liquid, then liquid is driven into the pores because of capillary pressure under appropriate conditions ($\theta < 90°$).

Before proceeding with a discussion of capillary wetting measurements and results, parameters such as viscosity, density, and surface tension need to be addressed. Relevant densities used in the analysis of capillary wetting data for epoxy−nanoclay mixtures are summarized in Supporting Information. Differences in densities of these material systems were observed to be very small. This was attributed to the small differences in the nanoclay loadings and probable experimental errors during meniscus readings. The results of room-temperature viscosity measurements of reactive nanoreinforced epoxy systems are presented in Figure 3 as a function of shear rate and time. It is also important to note that this particular epoxy-curative system was designed for final curing at elevated temperatures (i.e., first curing at 80 °C for 2 h followed by postcuring at 125 °C for 3 h). The viscosities appear to be pseudoplastic at low shear rates and then become nearly invariant in the shear rate range of 1×10^{-1} to 1×10^{2} s^{-1} examined. As anticipated, viscosity increases with increasing levels of nanoclay. It is important to note the there is very little, if any, viscosity increase over the time frame ($\sim 1 \times 10^3$ s) used to collect the rheology data and this approximates the region over which capillary wetting data were also collected. For the calculation of wetting rates, viscosities averaged over a shear rate range of 1×10^{-1} to 1×10^{2} s^{-1} were used in eq 1.

Surface tensions of both epoxy and reactive epoxy-curative−nanoclay mixtures are summarized in the Supporting Information. These results served to emphasize the

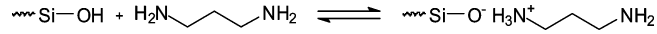

FIGURE 4. Schematic representation of the possible interactions between amine molecules and ionizable groups such as Si−OH groups available on a clay surface.

relative importance of competition between chemical reactions of amine in the bulk of the epoxy resin mixtures and surface excess of amine at the epoxy/air interface on surface tension reduction. In the case of the epoxy-curative mixtures, the amine molecules adsorbed at the epoxy−air interface were found to lower the surface tension of epoxy mixtures, as the measured surface tension of the diamine curative is much smaller than that of neat epoxy. The diamine curing agent caused an immediate 25% reduction in surface tension of the epoxy. The surface tension of epoxy-nanoclay mixtures, without any curative, was observed to be ~10% lower than that of neat epoxy. This is attributed to surface activity of the octadecylamine surfactant, a monoamine constituting ~25−30 wt % of the montmorillonite nanoclay. Beyond 2 wt % nanoclay, no further decrease in surface tension of the epoxy mixture was observed. This indicated that octadecylamine, released from the nanoclay, had reached a saturation concentration at the epoxy−air interface.

Another interesting result of surface tension measurements was that the addition of only 2 wt % nanoclay to the epoxy-curative mixtures did not change the surface tension, whereas that of 4 wt % nanoclay led to a 12% increase in the surface tension. This can be explained by a reduction in the surface excess of curative at higher nanoclay loading levels. In fact, it is well-known that most minerals, such as nanoclays, have negative zeta potentials due to the presence of ionizable groups (32, 33) such as $Si{-}OH \leftrightarrow Si{-}O^- + H^+$. Therefore, they could react (moderately acidic silanol/relatively basic amine) with the curing agent in an acid/base reaction on one extreme or simply form a hydrogen-bonded complex on the other as described in Figure 4. The consumption of curative in such a reaction would have a very negative free energy of adsorption and could reduce surface excess of diamine substantially. In essence, there is a competition between octadecylamine compatibilizer and amine curative for the clay and resin-air interfaces, as depicted in Figure 5. This competition could be explored through a surface tension isotherm measurement in the presence of varying amounts of nanoclay and curative. Ultimately, thermodynamics determine the partition coefficients. Given the time frame of the experiments and making some assumptions regarding adsorption isotherms based on concentration and diffusional kinetics, the system is likely to be close to equilibrium during examination. Increasing the amount of nanoclay can sequester larger quantities of amine curative and results in less amine being able to reach the surface at the same levels of added curative. Nanoparticles have large surface area/mass ratios and are capable of sequestering large amounts of surface active material. Hence, a reduction in the surface excess of amine would lead to higher surface tension in the case of epoxy-curative 4 wt % clay mixtures. Such events could also

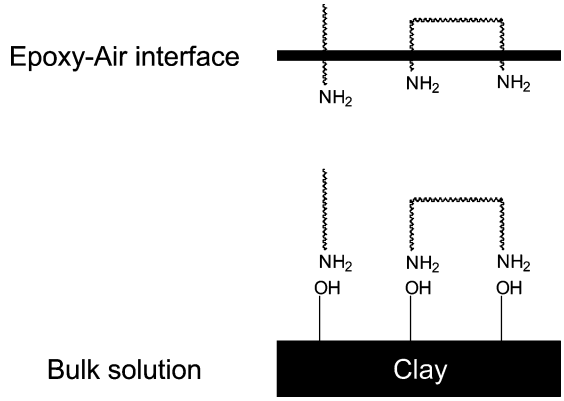

FIGURE 5. Schematic representation of the competition of amine molecules between the epoxy−air interface and clay surface.

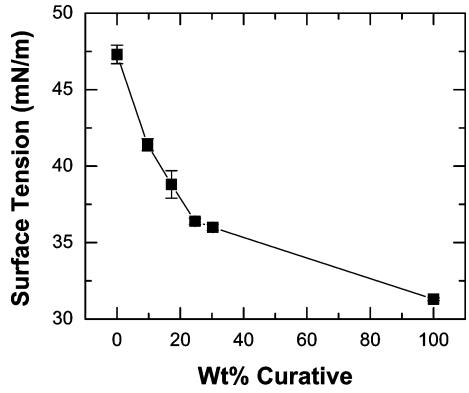

FIGURE 6. Surface tension isotherm of epoxy-curative mixtures.

change the effective level of curative and alter the state of cure in nanoclay-reinforced epoxy composites.

In an attempt to verify that increases in surface tension of epoxy mixtures at higher nanoclay addition levels are relevant to wetting, additional surface tension measurements of epoxy systems were conducted at various stoichiometric ratios of epoxy-to-curative in the absence of nanoclay. The surface tension isotherm is plotted in Figure 6. As expected, the surface tension of epoxy was found to decrease as a function of the curative amount. These results confirmed that the observed increases in surface tension at high nanoclay addition levels are related to the presence of nanoclay. The results of these surface tension measurements served to support the conclusion that curative could adsorb on the nanoclay surface and thus reduce its effective concentration and ability to lower the surface tension of the epoxy-curative−nanoclay mixtures.

The capillary experiments in this research were conducted with reactive epoxy-nanocomposite mixtures as well as with neat silicone oil and nanoreinforced silicone oil mixtures. To understand the effects of nanoreinforced epoxy systems in different flow regions, we conducted capillary wetting experiments with both glass fiber tow and fabric samples. As hydraulic constants, R_c, of test samples were needed for the evaluation of wetting properties of both fabric and tow samples with reactive epoxy−nanoclay systems, silicone oil−clay experiments were conducted initially. To ensure complete wetting (i.e., cos $\theta = 1$) of the tow and fabric samples, it was essential to use a low surface tension

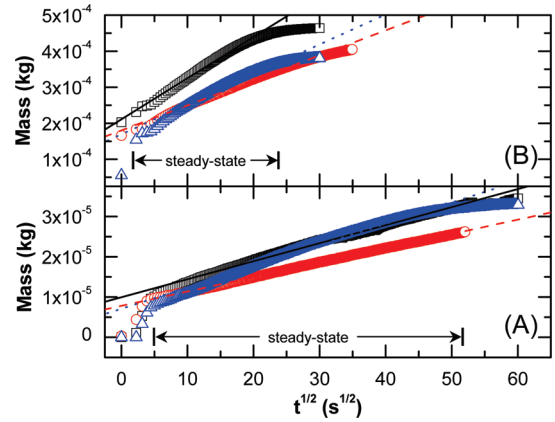

FIGURE 7. Capillary wetting rates of silicone oil−clay systems for tow wetting with (a) 0 (□), 2 (○), and 4 wt % (△) clay and for fabric wetting with (b) 0 (□), 2 (○), and 4 wt % (△) clay, along with linear least-squares fits over the steady-state wetting region.

fluid such as silicone oil. Capillary wetting measurements of nanoreinforced silicone oil mixtures were not only useful for determining hydraulic constants but also helpful for isolating the effect of nanoclay from that of curative. Silicone oil−nanoclay viscosities and densities are given in the Supporting Information (Table SI2).

The effects of different nanoclay loading levels on the capillary wetting of tow and fabric samples with silicone oil systems are plotted in Figure 7. A careful observation shows that the impregnation of both fabric and tow samples with silicone oil appears to occur fast initially. These initial impregnation rates are considered unusually high and are unreasonable considering the material properties. This abnormality can be attributed to "edge" effects as the test liquid wetted a sample and mass increased quickly throughout the edge region of the tow or fabric samples. The edges of both glass fabric and tow samples contacting the wetting liquid first are more "jagged" and irregular than the remaining portion of the fabric or tow. This can be seen at the top of Figure 2A. Undoubtedly, the fabric in Figure 2A has a much more "open" structure, resulting in a larger effective capillary radius (hydrodynamic volume). According to the Washburn equation, the wetting rate, *inter alia*, is directly proportional to the capillary radius. Another source of error could arise from the motion of fibers at the beginning of capillary measurements. Although it was assumed that the fibers remained stationary during impregnation, this assumption may be questionable as surface tension forces may induce fiber motion at the beginning of the measurements. Hence, the initial part of the wicking experiments can be considered as unsteady-state and cannot represent the tow internal structure or capillarity. The region of data chosen for analysis of fabric wetting properties by the Washburn equation is over the "steady-state" "region" (steady-state $t \gtrsim 25$ s) until wetting terminates because of the countering influence of gravity. Approximate steady-state regions are indicated in Figure 7. The low time limit of the steady-state region was chosen immediately after the initial, rapid mass increase described above. Linear least-squares fitting of the data was performed over the steady-state region such that the correlation coefficient in the fit was >0.99. The wetting data

Table 1. Effect of Nanoclay Loading on the Silicone Oil–Fabric and Silicone Oil–Tow Wetting Properties

wt % clay	R_c $(cm^5)_{Tow}$	R_c $(cm^5)_{Fabric}$
0	$(1.36 \pm 0.358) \times 10^{-9}$	$(1.10 \pm 0.215) \times 10^{-6}$
2	$(1.23 \pm 0.655) \times 10^{-9}$	$(3.62 \pm 1.30) \times 10^{-7}$
4	$(1.90 \pm 0.292) \times 10^{-9}$	$(7.99 \pm 1.92) \times 10^{-7}$

from three independent experiments for each nanoclay loading were then used for subsequent calculations of capillary wetting parameters and R_c in particular.

The results of silicone oil–nanoclay wetting experiments for fabric and tow samples are presented in Table 1. A comparison of hydraulic constants calculated via the Washburn equation using the corresponding wetting rates obtained from the slopes of steady-state regions of wetting experiments indicated that both hydraulic constants and wetting rates of tow samples were approximately two-orders of magnitude lower than those of fabric. The fabric samples, having a more "open" structure than the tow samples due to the presence of both inter- and intratow regions, are expected to have a larger capillary radius and a higher value of the hydraulic constant. This, in turn, gives rise to higher wetting rates in fabric, as the wetting rate is directly proportional to the hydraulic constant according to eq 1.

Another interesting result of silicone oil experiments was that there was a decrease in hydraulic constants of both fabric and tow samples at 2 wt % nanoclay loadings as shown in Figure 8. This is explained by the competition between wetted area, A, and capillary radius, r. The hydraulic constant, R_c, is proportional directly to both of these variables as given in eq 2. At low nanoclay loading levels (such as 2 wt %), the surface area of nanoclay particles wetted by silicone oil was low. In addition, much less aggregation of nanoclay particles is expected based solely on the concentration dependence of aggregation. The determination of the actual extent of aggregation remains for future investigation. This lessened the possibility of a significant increase in wetted area, A, even if there can be some "clogging" of pores of a fabric or tow by the nanoparticle. The increase in wetted areas is not expected to be as high as the decrease in capillary radius, r, at low loadings of nanoclay. Thus, the decrease in R_c at low additional levels

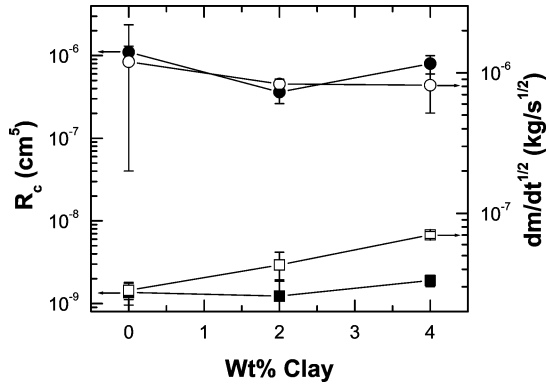

FIGURE 8. Effect of nanoclay addition on the hydraulic constant, R_c (■ tow, ● fabric), and capillary wetting rate, $dm/dt^{1/2}$ (□ tow, ○ fabric) using the silicone oil systems.

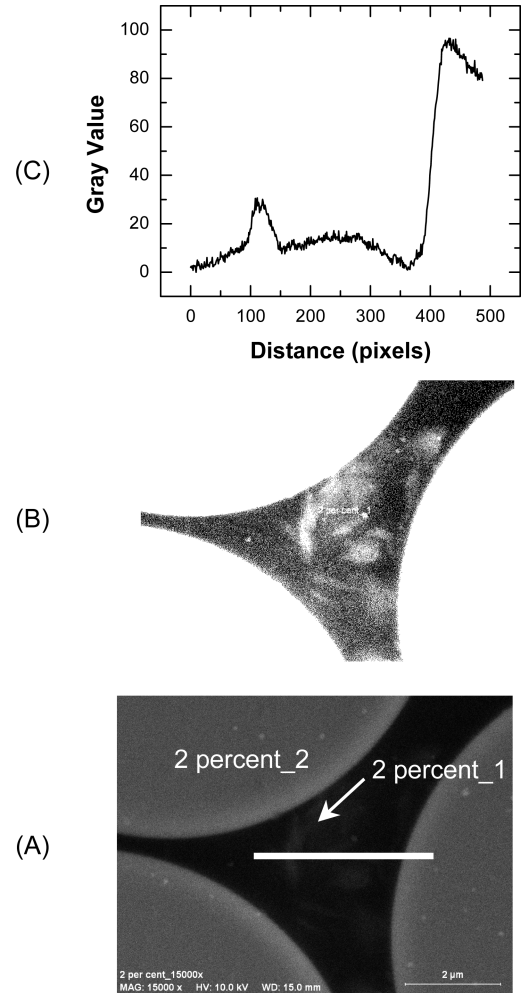

FIGURE 9. SEM image of an intertow region of a cured epoxy–2 wt % nanoclay–fiber glass fabric. (A) The region designated "2 percent_2" is a single fiber, whereas the region labeled "2 percent_1" is believed to be a nanoclay aggregate or tactoid. (B) Enhanced contrast version of A. (C) Gray scale vs distance plot from the white line shown in A. Background normalized to zero on a gray scale.

of nanoclay is attributed mainly to a decrease in hydraulic radius due to the presence of nanoclay. Such a situation, in turn, causes a decrease in the wetting rates. On the other hand, increases in R_c at higher loading of nanoclay, such as 4 wt %, can be explained on the basis of higher surface area of clay particles that was wetted by silicone oil and the likelihood of more aggregation of clay particles. The increase of wetting rate is more pronounced in the case of tow as would be expected on the basis of the capillary radius being smaller for tow than fabric. From the definitions given in eq 2, R_c is linear with r but quadratic with A; therefore, the effect of $\Delta A/\Delta r$ will be magnified with increased surface area because of aggregation at higher nanoclay loading. This factor complicates capillary wetting experiments for binary systems (i.e., two wetting surfaces), such as silicon oil–nanoclay systems. A similar anomaly in wetting rates with nanoclay loading is also noted, vide infra, during capillarity wetting measurements of single tow and fabric samples with epoxy-curative–nanoclay systems. These results appear to be reproducible.

Table 2. EDS Elemental Composition Data Collected from Different Sections of a Molded Epoxy−Clay−Glass Fiber Sample

	at %			
sample	Na	Mg	Al	Si
clay tactoid/aggregate[a]	0	5.30	22.9	71.8
NANOCOR I30-E nanoclay[b]	0.73	4.78	26.0	68.5
glass fiber[c]	1.30	4.41	15.9	78.0

[a] "2 percent_1" area in Figure 9 A. [b] Pure nanoclay material. [c] "2 percent_2" area in Figure 9A.

The presence of nanoclay aggregates or tactoids in the fabrics impregnated with epoxy−nanoclay was investigated by SEM and EDS. Figure 9 shows an SEM photograph of a cross-section of a fabric cured with epoxy−2 wt % nanoclay. A comparison of elemental analysis data for pure nanoclay, the apparent nanoclay aggregate or tactoid and glass fiber is provided in Table 2. Carbon and oxygen contributions were omitted from the calculation because of the epoxy background signal from the potting medium and the conductive carbon coating. Although the structure in the region between the fiber tows in this image suggested to be a nanoclay aggregate may be somewhat equivocal, its dimensions are much larger than those expected for a single nanoclay platelet. The structure does not resemble a symmetrical fiber and its cross-section is on the order of 2 μm. A comparison of its elemental composition shows a much closer match to pure nanoclay than to a glass fiber. It is important to note that at ~2 μm in cross-section, nanoclay aggregates may be larger than intertow spaces and capable of impeding capillary flow while providing additional and different surface area, vide supra, to be wetted.

Similar wetting experiments were also conducted with reactive epoxy−nanoclay mixtures that were the main interest of this research. The effects of different nanoclay loading levels on the capillary wetting of tow and fabric samples with epoxy-curative systems are shown in Figure 10. Wetting rates of epoxy-curative−nanoclay tow and fabric systems are given in Tables 3 and 4, respectively. Figure 10 reveals that there are two major flow regimes during which

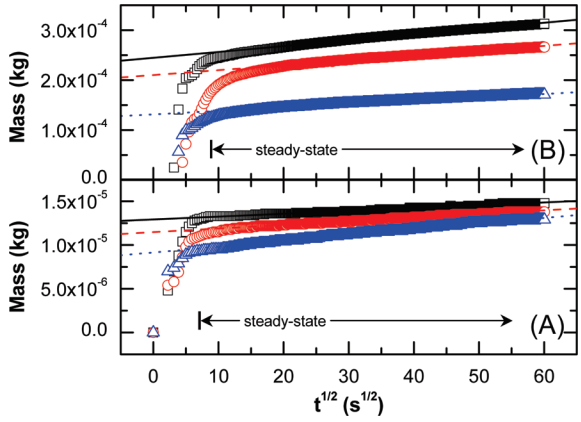

FIGURE 10. Capillary wetting rates of epoxy-curative−clay systems for tow wetting with (A) 0 (□), 2 (○), and 4 wt % (△) clay and for fabric wetting with (B) 0 (□), 2 (○), and 4 wt % (△) clay, along with linear least-squares fit over the steady-state wetting region.

Table 3. Effect of Nanoclay Loading on the Epoxy-Curative Tow Wetting Properties

wt % clay	wetting rate, $dm/dt^{1/2}$ (kg/s$^{1/2}$)	wetting Rate, dh/dt (m/s)[a]	Ca_{Tow}
0	$(2.83 \pm 0.439) \times 10^{-8}$	$(3.2 \pm 0.58) \times 10^{-7}$	$(5.2 \pm 1.2) \times 10^{-6}$
2	$(4.29 \pm 1.14) \times 10^{-8}$	$(3.9 \pm 1.9) \times 10^{-7}$	$(7.7 \pm 4.0) \times 10^{-6}$
4	$(7.03 \pm 0.294) \times 10^{-8}$	$(7.9 \pm 1.9) \times 10^{-7}$	$(1.4 \pm 0.41) \times 10^{-5}$

[a] Adjusted for tow dimensions: 0.52 ± 0.05 mm (thickness) × 2 ± 0.05 (width) mm × 120 ± 0.05 mm (length) using $h = m/(\rho w_{tow} t_{tow})$, where m is mass, ρ is liquid density, w_{tow} is tow width, and t_{tow} is tow thickness.

Table 4. Effect of Nanoclay Loading on Epoxy-Curative Fabric Wetting Properties

wt % clay	wetting rate, $dm/dt^{1/2}$ (kg/s$^{1/2}$)	wetting rate, dh/dt (m/s)[a]	Ca_{Fabric}
0	$(1.20 \pm 0.143) \times 10^{-6}$	$(1.2 \pm 0.015) \times 10^{-6}$	$(1.9 \pm 0.12) \times 10^{-5}$
2	$(8.33 \pm 0.523) \times 10^{-7}$	$(8.9 \pm 0.23) \times 10^{-7}$	$(1.7 \pm 0.13) \times 10^{-5}$
4	$(8.17 \pm 2.27) \times 10^{-7}$	$(8.2 \pm 2.8) \times 10^{-7}$	$(1.5 \pm 0.56) \times 10^{-5}$

[a] Adjusted for fabric dimensions: 0.52 ± 0.05 mm (thickness) × 20 ± 0.05 (width) mm × 50 ± 0.05 mm (length) using $h = m/(\rho w_{fabric} t_{fabric})$, where m is mass, ρ is liquid density, w_{fabric} is fabric width, and t_{fabric} is fabric thickness.

the impregnation rates of viscous reactive epoxy mixtures were substantially different. Similar to the silicone oil−nanoclay wetting measurements plotted in Figure 7, the wetting rates ($dm/dt^{1/2}$) of fabric samples were observed to be approximately an order-of-magnitude faster than those of tow samples. This is attributed to the availability of much larger wetted areas in the fabric samples than those in the single tow samples. The greater wetted areas in fabric are explained by the presence of intertow regions in addition to the clay surface areas and the areas of the walls of fibers in the intratow regions.

The preceding discussion of capillary wetting rates via eq 1 is predicated on the assumption that ideal Washburn-type behavior is exhibited. Popescu et al. (34) proposed a critical empirical parameter, k_0, to predict flow conditions that will cause deviations from ideal Washburn capillary wetting behavior.

$$k_0 = \frac{V\gamma_0}{v_0\gamma} \tag{3}$$

$$V = \frac{\rho g r^2}{8\mu} \tag{4}$$

In eqs 3 and 4, γ_0 is a term proportional to thermal energy, v_0 is a velocity determined by molecular properties of the substrate, γ is surface tension, ρ is density, g is the gravitational constant, r is the capillary radius, and μ is dynamic viscosity. For $k_0 > 1$, deviations from Washburn behavior were expected. In the present study, estimates gave $k_0 \leq 1$, and accordingly, minimal deviations from ideal Washburn behavior are expected.

In a binary system like the one in this study, decoupling of the variables such as contact angle and hydraulic constant,

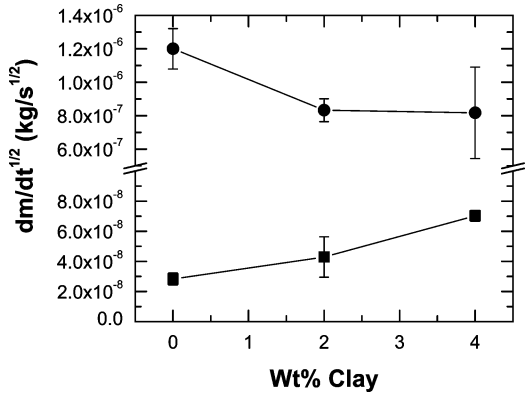

FIGURE 11. Effect of nanoclay concentration on wetting rate of tow (■) and fabric (●) structures using the epoxy-curative−nanoclay system.

R_c in eq 1 is difficult, as a change in one variable results in a change in the other. In addition, deconvolution of changing wetted areas, A, and capillary radius, r, from R_c with the addition of nanoclay may not be practical. As surface tension and viscosity are the other two variables used in eq 1, their effects on wetting rates have to be examined for a complete analysis of such binary systems. The wetting rates are expected to increase with an increase in surface tension and a decrease in viscosity of the wetting fluids according to the Washburn equation (eq 1). Surface tension values of nanoclay-reinforced epoxy systems were observed to increase with an increase in nanoclay content. This implies an increase in wetting rates based on the Washburn equation (eq 1). Although this expectation was confirmed in the case of tow-wetting experiments, one should also remember that an increase in surface tension usually results in an increase in contact angle. As surface tension and contact angles have opposite effects on wetting rates, their contributions may cancel under appropriate circumstances. Another interesting finding of this study was that, despite the fact that the viscosity of nanoreinforced epoxy systems was observed to increase with the addition of nanoclay, it was found that wetting rates observed in tow and fabric structures with nanoclay-reinforced reactive epoxy mixtures were of opposite sign as shown in Figure 11. Viscosities of reactive nanoreinforced epoxy mixtures were expected to be the same under identical experimental conditions whether the mixtures were used to wet a tow or a fabric structure. On the basis of experimental observation, it was concluded that increases in wetting rates of a single tow and decreases in the wetting rates of a fabric cannot be correlated with increases in viscosity in the presence of nanoclay.

Further analysis of the relative importance of interfacial forces to viscous forces during capillary wetting of single tow and fabric structures with nanoclay−reinforced epoxy mixtures can be made using dimensionless fluid dynamics parameters. Raw data readings of fluid mass gain as a function of t were recast into fluid impregnation or spreading heights, h. This was performed using the experimental mass gain data by converting to volume using the liquid density and then equating to the linear dimension of height by dividing by the product of fabric or tow width and thickness. The comparisons of the spreading heights of epoxy mixtures at different nanoclay loadings are illustrated separately in the Supporting Information (Figures SI1 and SI2). A careful observation of Figure 10 indicates the unusually high initial impregnation rate regions due to the edge effects similar to those observed in silicone oil measurements. The steady-state regions used for analysis are indicated in Figure 10 (steady state $t \gtrsim 100$ s). Using the slopes of the steady-state regions of h *vs* t ($t \gtrsim 100$ s), a further analysis of capillary flow with two dimensionless numbers, capillary number, *Ca*, and Reynolds number, *Re*, was performed. Data from three independent wetting experiments were used and averaged for analysis of wetting rates and, subsequently, for *Ca* and *Re*.

It must be noted that capillary wetting experiments were conducted under axial impregnation conditions without the influence of any RTM mold. Capillary numbers evaluated under these conditions should give a reasonable estimate of flow parameters based solely on the fabric or tow structures. The capillary number, $Ca = \mu v/\gamma$, is a measure of the ratio of viscous to capillary forces during flow, where μ is dynamic viscosity, v is fluid velocity, and γ is surface tension (35). The values of *Ca* for tow and fabric are reported in Tables 3 and 4, respectively. In both cases, it is seen that $Ca \ll 1$. Because the capillary number $\propto \mu/\gamma$, the relative changes in these two quantities will determine the value of *Ca*. The results of capillary wetting experiments, shown in Figure 10, suggest that steady-state wetting is achieved over a time scale of $t > 100$ s. The surface tension data indicate a substantial increase of epoxy-curative surface tension with the addition of clay. Because $\Delta\mu/\Delta\gamma < 1$, the capillary number is reduced. The Washburn equation (eq 1) suggests that the capillary wetting rate, $dh/dt \propto \gamma/\mu$ and, as a consequence, an increase in μ/γ ratio results in a smaller rate and this was, indeed, observed in experimental results. As capillary numbers were observed to be $\ll 1$, it was concluded that flow was mainly governed by surface tension forces during capillary wetting of both single tow and fabric samples.

The Reynolds number, *Re*, is a measure of inertial to viscous effects during flow and is defined as

$$Re = \frac{\rho V D}{\mu} \tag{5}$$

where ρ is density, V is velocity, D is effective diameter, and μ is dynamic viscosity. Using the experimentally determined steady-state $(dh/dt)_{tow}$ values and intratow gap distances of 1×10^{-5} m along with some typical density and viscosity values, the Reynolds number of the intratow regions was estimated to be in the range of 1×10^{-9}, whereas the *Re* of fabric structures was estimated to be $\sim 1 \times 10^{-9}$ to 1×10^{-8}. Because the Reynolds number is $\ll 1$, it was concluded that these types of capillary flows were in the creeping flow regime. Thus, dispersion of nanoclay aggregates formed during capillary wetting conditions was not possible due to induced flow. Even under "forced" wetting conditions during RTM of the same type of fabric structures with much larger

flow rates, Reynolds numbers were estimated to be $\sim 1 \times 10^{-2}$, implying that creeping flow conditions still prevailed.

Assuming that fabric structures comprised tows with a hexagonal, close-packed arrangement of fibers and using an approximate glass fiber diameter of 13 μm (given by the manufacturer), the area between fibers in a tow (i.e., intratow area) was approximated with an equilateral triangle area of $\sim 1.1 \times 10^7$ nm^2. This gives an approximate capillary gap distance of 3.3 μm between fibers in a tow. Knowing that the average size of an individual nanoclay platelet was ~ 1 μm $\times$ 1 μm $\times$ 1 nm and the average size of tactoids, i.e., aggregates of hundreds of individual nanoclay platelets, was in the range of several micrometers, large size tactoids potentially had the opportunity to block intratow capillaries (see, for example, Figure 9) during flow in the absence of high shear. Using the experimentally determined impregnation rates of tow (Table 3) along with the available gap distance of 3.3 μm between individual fibers in a tow (i.e., intratow), tow shear rates were estimated to range from 6.1×10^{-3} s^{-1} to 0.28 s^{-1} during capillary wetting. Likewise, knowing that the dimensions of intertow spacing were approximately 2 orders of magnitude larger than intratow capillaries and experimentally determined impregnation rates of fabrics presented in Table 4 were only 1−5 times larger than those of tow (intratow), shear rates in fabric structures were expected to be less than those in tows by at least by 2 orders of magnitude. These results indicate that shear rates estimated in tow and fabric structures subjected only to capillary flow conditions were trivial. This implies that the possibility of any tactoid dispersion by the induced flow and shear was minimal.

It was reported by several researchers (14, 15, 28) that capillary forces have a substantial influence on the uniformity of micro- and macroflows that exist during RTM. Voids trapped during the mold-filling stage of the RTM are also believed to be the consequence of nonuniform micro- and macroflows. Microflows between filaments in a tow are driven by both capillary forces and injection pressure, whereas macroflows between fiber tows are driven mainly by injection pressure. Capillary flow in fiber tows is usually observed at low filling velocities when the microflow in the fiber tows precedes macroflow due to capillary effects. In such cases, macro-voids may be trapped between fiber tows. Thus, there is a critical capillary number range below which severe void problems can be observed during RTM. Although a critical capillary number of 2.5×10^{-3} was reported for RTM applications by Chang (28), Young (15) indicated a critical capillary number range of 1×10^{-4} to 2×10^{-4}. In any event, a $Ca \ll 1$ indicates that capillarity dominates over inertia in governing flow in the fabric or tows. Considering the fact that capillary numbers of the reactive epoxy−nanoclay mixtures were found to be as low as $\sim 1 \times 10^{-6}$, formation of macrovoids in the epoxy−nanoclay composites is expected. Indeed, examination of the performance of the RTM process and the possibility of void formation in RTM was supported these results and will be communicated separately.

CONCLUSIONS

Capillary wetting measurements were performed on a biaxially-oriented glass fabric and single tow samples comprising the fabric following the Washburn capillary wetting theory. Test fluid systems of silicone oil−nanoclay and epoxy-curative−nanoclay were investigated. The silicone oil measurements were first run to determine the relevant hydraulic constants, R_c, using the Washburn equation (eq 1) because the surface tension of silicon oil was low enough to ensure a contact angle = 0 against fabric. As anticipated, flow rates and hydraulic constants for fabric were determined to be 1−2 orders of magnitude larger than those for a single tow alone. This is based simply on a much larger capillary radius in fabric compared to a single tow. The silicone oil−nanoclay wetting experiments provided some unusual results. For both fabric and tow, there is a decrease in hydraulic constant and wetting rate at the 2 wt % nanoclay level followed by an increase at the 4 wt % level. These results are attributed to the definition of R_c given in eq 2 and the fact that a fabric or tow and nanoclay system is a binary system such that each system has its own surface area to be wetted and contact angle. Surface tensions of epoxy-curative mixtures were found to decrease with increasing curative level. Interestingly, surface tension of epoxy-curative−nanoclay mixtures increased with an increase in nanoclay content. This is attributed to the ability of nanoclay particles with large surface areas to sequester diamine curative and to prevent the reduction of surface tension. Capillary wetting rate data was also used to estimate capillary and Reynolds numbers. The values of *Ca* for fabric and tow using the epoxy-curative−nanoclay mixture were $\sim 1 \times 10^{-5}$ and 1×10^{-6}, respectively, indicating in both cases that flow was dominated by interfacial tension. The values of *Re* for fabric and tow were in the range of 1×10^{-8} to 1×10^{-9} and 1×10^{-9}, respectively. Shear rates estimated for intratow flow were in the range of 1×10^{-3} to 1×10^{-1} s^{-1}. The Reynolds numbers and shear rates in these ranges indicated the absence of significant dispersion of nanoclay aggregates and substantiate the existence of nanoclay aggregates. In summary, nanoclay-reinforced systems offer significant perturbations to simple capillary wetting predicted by the Washburn equation.

Acknowledgment. The authors thank DNV Research & Innovation for making the SEM and energy-dispersive spectrometer analysis of epoxy−nanoclay samples possible.

Supporting Information Available: Summary of density and surface tension measurements of various reactive and unreactive epoxy−nanoclay mixtures table; summary of viscosity and density values for silicone oil−nanoclay mixtures table; impregnation rates of epoxy-curative−nanoclay tow and fabric figures (PDF). This material is available free of charge via the Internet at http://pubs.acs.org.

REFERENCES AND NOTES

(1) Advani, S. G. *Flow and Rheology in Polymer Composites Manufacturing*; Elsevier: Amsterdam, 1994.
(2) Carrado, K. A. Polymer−Clay Nanocomposites. In *Advanced Polymeric Materials: Structure Property Relationships*; Shonaike,

G. O., Advani, S. G., Eds.; CRC Press: Boca Raton, FL, 2003; Chapter 10.
(3) Advani, S. G.; Sozer, M. Liquid Molding of Thermoset Composites. In *Comprehensive Composite Materials*; Kelly, A., Zweben, C., Eds.; Elsevier Science: Amsterdam, 2003; Vol. 2, Chapter 2.23.
(4) Boogh, L.; Mezzenga, R. Processing Principles for Thermoset Composites. In *Comprehensive Composite Materials*; Kelly, A. Zweben, C., Eds.; Elsevier Science: Amsterdam, 2000; Vol. 2, Chapter 2.19.
(5) Cai, Z. *J. Compos. Mater.* **1992**, *26*, 1310.
(6) Cai, Z. *J. Compos. Mater.* **1992**, *26*, 2606.
(7) Fan, Z.; Hsiao, K.-T.; Advani, S. G. *Carbon* **2004**, *42*, 871–876.
(8) Haque, A.; Shamsuzzoha, M.; Hussain, F.; Dean, D. *J. Compos. Mater.* **2003**, *37*, 1821.
(9) Thostenson, E. T.; Chou, T.-W. *Carbon* **2006**, *44*, 3022.
(10) Hamidi, Y. K.; Aktas, L.; Altan, M. C. *J. Thermoplast. Compos. Mater.* **2008**, *21*, 141.
(11) Kornmann, X.; Rees, M.; Thomann, Y.; Necola, A.; Barbezat, M.; Thomann, R. *Compos. Sci. Technol.* **2005**, *65*, 2259–2268.
(12) Chowdhury, F. H.; Hosur, M. V.; Jeelani, S. *Mater. Sci. Eng., A* **2006**, *421*, 298–306.
(13) Chowdhury, F. H.; Hosur, M. V.; Jeelani, S. *J. Mater. Sci.* **2007**, *42*, 2690–2700.
(14) Patel, N.; Rohatgi, V.; Lee, L. J. *Polym. Eng. Sci.* **1995**, *35*, 837.
(15) Young, W. B. *J. Compos. Mater.* **1996**, *30*, 1191.
(16) Bickerton, S.; Advani, S. G. *Compos. Sci. Technol.* **1997**, *57*, 23.
(17) Binetruy, C.; Hilaire, B.; Pabiot, J. *J. Compos. Mater.* **1998**, *32*, 223.
(18) Choi, M. A.; Lee, M. H.; Chang, J.; Lee, S. J. *J. Non-Newtonian Fluid Mech.* **1998**, *79*, 585.
(19) Lekakou, C.; Johari, M. A. K. B.; Bader, M. G. *Polym. Compos.* **1996**, *17*, 666.
(20) Nielsen, L. E. *J. Macromol. Sci., Part A: Pure Appl. Chem.* **1967**, *5*, 929.
(21) De Parseval, Y.; Pillai, K. M.; Advani, S. G. *Transp. Porous Media* **1997**, *27*, 243.
(22) Wang, J. T.; Wu, C. H.; Lee, J. L. *Polym. Compos.* **1994**, *15*, 278.
(23) Synytska, A.; Michel, S.; Pleul, D.; Bellmann, C.; Schinner, R.; Eichhorn, K.-J.; Grundke, K.; Neumann, A. W.; Stamm, M. *J. Adhes.* **2004**, *80*, 667.
(24) Chwastiak, S. *J. Colloid Interface Sci.* **1973**, *42*, 298.
(25) Washburn, E. W. *Phys. Rev.* **1921**, *17*, 273.
(26) Pillai, K. M. *Composites, Part A* **2002**, *33*, 1007.
(27) Foister, R. T. *J. Colloid Interface Sci.* **1984**, *99*, 568.
(28) Chang, C. Y. *J. Reinf. Plast. Compos.* **2003**, *22*, 1003.
(29) Zuidema, H. H.; Waters, G. W. *Ind. Eng. Chem.* **1941**, *13*, 312.
(30) Lee, H.; Neville, K. *Handbook of Epoxy Resins*; McGraw-Hill: New York, 1982.
(31) Chen, D.; McMorran, D. *Am. Lab.* **1999**, 35.
(32) Kosmulski, M. *J. Colloid Interface Sci.* **2002**, *253*, 77.
(33) Delgado, A.; Gonzalez-Caballero, F.; Bruque, J. M. *J. Colloid Interface Sci.* **1986**, *113*, 203.
(34) Popescu, M. N.; Ralston, J.; Sedev, R. *Langmuir* **2008**, *24*, 12710.
(35) Tucker, C. L., III; Dessenberger, R. B. Governing equations for flow and heat transfer in stationary fiber beds. In *Flow and Rheology in Polymer Composites Manufacturing*; Advani, S. G., Ed.; Elsevier: Amsterdam, 1994; p 257.

AM900179X